Quantitative Studies of Meteosat Water-Vapor Channel Data

M. M. POC, M. ROULLEAU, N. A. SCOTT AND A. CHEDIN

Laboratoire de Météorologie Dynamique, Ecole Polytechnique, 91128 Palaiseau Cedex, France

(Manuscript received 17 October 1979, in final form 29 March 1980)

ABSTRACT

In this paper, quantitative studies of water vapor Météosat imagery, based on an accurate transmittance and radiance model are described. Using conventional radiosonde data, a linear relation between cloudless radiances and digital counts is obtained. It is shown that the distribution with altitude of the peak contribution to the radiances varies from about the 550 mb level to about the 450 mb level for pictures acquired in July over the western part of Europe and Mediterranean Sea. The influence of the temperature profile on the altitude of the maximum contribution layer is pointed out. A relation between the radiative field and the water vapor mass above the 600 mb level is found.

1. Introduction

Water vapor imagery is a subject of interest since it provides additional information to the usual meteorological data from satellites. Although interpretation of these radiometric data is in its early stages, water vapor channel observations have been made for some time from polar orbital satellites, and qualitative meteorological results deduced from this imagery. As early as 1961, Möller pointed out that the radiances within the 6.3 μm band of water vapor can be related to the mean relative humidity of the troposphere. Möller and Raschke (1963)[1] and Raschke and Bandeen (1967), using coordinated infrared radiometric measurements in the two spectral intervals (8–13 and 5.7–6.9 μm) developed and employed a "humidity diagram" to infer the relative humidity of the upper troposphere over large sections of the world. These studies involved not only atmospheric moisture measurements but also tropospheric dynamics. Rodgers *et al.* (1976) used Nimbus-4 THIR 6–7 μm observations to complete the 500 mb humidity patterns deduced from conventional water vapor data. Steranka *et al.* (1973), using the same kind of data, suggested that the water vapor imagery could be used for deriving dynamic features over data-sparse regions in cloudless areas. More recently, an analysis of Nimbus-5 THIR 6–7 μm observations over the Mediterranean Sea showed that it should be possible to use imagery features over wet or dry regions as dynamical tracers in clear-sky conditions (Roulleau, 1978). In all these studies, the altitude of the phenomena observed on the water vapor picture is defined as being broadly between the 500–250 mb levels, though Shenk and Rodgers (1974),[2] studying satellite views of Hurricane Camille, suggested that the information from the water vapor channels offers a possible method for inferring subsidence in clear air in the middle and upper troposphere.

Now Meteosat provides water vapor pictures every half-hour from the same points of the earth. Thus, quantitative studies relating spatially and temporally varying patterns can be deduced from radiometric data, provided that accurate synthetic computations are carried out. For that purpose, we used a line-by-line model for generating atmospheric transmissions and radiances in the spectral range of the water vapor channel.

This approach was first tested by studying an image acquired from the THIR experiment flown aboard the sun-synchronous Nimbus-5 meteorological satellite which water vapor channel calibration was known. Then we realized an analysis of water vapor Meteosat pictures from which we deduced three types of information:

- The relation between cloudless radiances and digital counts
- The distribution with altitude of the integrated outgoing radiance sensed by the water vapor channel
- The relation between the radiative field and the water vapor mass above the 600 mb level.

[1] Möller, F., and E. Raschke, 1963: Evaluation of TIROS-III radiation data. Interim Rep. No. 1, Meteorologisches Institut, Universität München, NASA Grant 305, 114 pp.

[2] Shenk, W. E., and E. B. Rodgers, 1974: Satellite views of Hurricane Camille. NASA Tech. Note TN 0-7547.

0021-8952/80/070868-09$06.25

2. Evaluation of synthetic transmittance and radiance

Determination of atmospheric transmittances and radiances is performed using the STRANSAC line-by-line model. This model has already been detailed in different references (Scott, 1974; Chedin *et al.*, 1978). The method is based on a direct integration in frequency and the use of the finestructure parameters of the absorbing gases. The spectral region of Meteosat water vapor channel is centered within the 6.3 μm absorbing band: 1342–1174 cm^{-1}. In this spectral interval, four gases absorb (H_2O, CO_2, CH_4, N_2O) but the absorption is mainly due to water vapor. Comparative radiance calculations were made taking into account either H_2O alone or the four absorbing gases. Results obtained using meteorological data from two model atmospheres showed no significant differences (<0.5%). The transmittances are evaluated with a frequency integration step equal to 2.5×10^{-3} cm^{-1}, which is the value of the Doppler half-width of the water vapor lines at the highest level of the atmosphere. The line shape profile is cut off beyond 600 half-widths from the line center. The atmosphere is divided into 20 layers with pressure levels ranging from 1000 to 5 mb. (A test realized with 30 layers showed no significant changes in the results). Each layer is characterized by a pressure, a temperature and a concentration which are the mean values of these parameters at the boundary levels of the layer. These layers are not uniformly distributed in order to achieve a better description of the region of interest. The radiance I, measured by the satelliteborne radiometer, is related to the optical path, that is to the temperature and the absorbing gas structure, through the radiative transfer equation, taking into account the filter response.

3. Response of Meteosat water vapor channel

An actual quantitative analysis of Meteosat water vapor data requires the WV channel calibration, that is, the relation between the digital counts of the signal received by the radiometer and the radiances or the equivalent blackbody temperatures. Until now, the European Space Operations Centre has published only a temporary calibration curve (Morgan, 1979).[3]

In order to test the method described in Section 2, a preliminary study of a Nimbus-5 THIR picture was made. This picture was acquired at 0000 GMT 9 January 1973. The interesting region was centered over France and the western part of the Mediterranean Basin. Using the meteorological data from cloudless soundings, the model described in Section 2 was used to calculate the values of the outgoing radiance in order to compare these with the values observed on the picture. This comparison was made possible because of the existence of the calibration curve of the 6–7 μm channel of the experiment (available in *The Nimbus-5 Users Guide*, NASA, 1972).[4] Results of the comparison are shown in Table 1 where I_{cal} is the calculated radiance value obtained with the model, I_{LMD} is the radiance observed on the Mercator projection of the picture obtained in the laboratory, I_{GSFC} is the radiance observed on the Mercator map acquired from the Goddard Space Flight Center.

TABLE 1. Comparison of calculated and observed THIR NIMBUS-5 radiances (asterisk indicates possible localization error). Units: W m^{-2} sr^{-1}.

Stations	I_{cal}	I_{LMD}	I_{GSFL}
Bordeaux	1.02	1.13	1.22
Brest	1.15	1.33	1.26
Gibraltar	1.10	0.76*	1.10
Lyon	1.11	1.14	1.18
Malte	0.85	0.70	0.74
Milan	1.11	1.08	1.08
Rome	0.94	0.92	0.89
Trappes	1.31	1.20	1.18
Udine	0.91	0.99	0.99

Once the validation of the method was effected, we were able to infer the response of Meteosat water vapor channel. We tried to establish the relationship between the radiance values calculated from atmospheric data and the numerical values measured in cloudless conditions on an image at definite geographical points.

We studied 14 and 16 July 1978 pictures at 1200 GMT in the geographical region between 30 and 55°N and between 20°W and 25°E, that is mainly the occidental part of Europe and Mediterranean Basin. Fig. 1 illustrates the picture of 14 July 1978 visualized from the digital data tapes in the three Meteosat channels: visible (Fig. 1a), window (Fig. 1b) and water vapor (Fig. 1c). On 16 July 1978 the image was quite similar.

These two cases were chosen because of special clear-sky conditions over a region where there is a sufficient number of conventional meteorological data available. The cloudless atmospheric data are obtained from the radiosoundings. Only soundings giving water vapor vertical distribution up to the 300 mb level were used. Above this level, humidity was extrapolated to conform to McClatchey's mid-latitude summer model atmosphere (1972).[5]

[3] Morgan, J., 1979: Meteosat 1. Calibration Rep., Issue 3. ESOC.

[4] *Nimbus-5 User's Guide*, 1972: Goddard Space Flight Center, Greenbelt, MD.

[5] McClatchey, R. A., R. W. Fenn, J. E. A. Selby, F. E. Voltz and J. S. Garing, 1972: Optical Properties of the atmosphere. AFCRL 72-0497.

(a)

(b)

(c)

FIG. 1. Pictures from Meteosat, 14 July 1978, 1200 GMT. (a) Visible channel. (b) Window channel. (c) Water vapor channel.

Meteosat is placed in geostationary position at 0° longitude, then, for the chosen geographical region, the zenith angles at the stations are rather large (~50°) and the ground resolution is ~8 km in the water vapor channel. The exact value of the angle was introduced in the model for each of the radiosounding stations. The stations are localized by means of an interactive computer system for image visualization. Landmarks are pointed from the corresponding picture in the visible channel and, using a navigation programme which takes into account the position parameters of the satellite, the stations are mapped with an accuracy lower than four pixels. The ground distance of four pixels is of about the mean horizontal trajectory of a radiosounding balloon ascending to the tropopause.

In July the detector of the radiometer was regulated at 90 K. The European Space Operations Centre provided us with the relative spectral response of the detector versus frequency only at 85 and 110 K as shown on Table 2. The apparatus function used in the radiance calculations was deduced from the 85 K data. This function is shown in Fig. 2. To keep a check on this apparatus function, the radiance values of the Planck temperatures were calculated and compared with the values published in Table 4 of the ESOC Calibration Report-Issue 3. Table 3 shows the good agreement of the results.

TABLE 2. Absolute spectral response of Meteosat WV channel: $\tau(\lambda)$ is the optical transmission, $r_T(\lambda)$ is the relative spectral response of the detector at the temperature T.

λ (μm)	$\tau(\lambda)$	$r_{85}(\lambda)$	$r_{110}(\lambda)$	$\tau(\lambda)r_{85}(\lambda)$	$\tau(\lambda)r_{110}(\lambda)$
5.48	0	0.96	0.95	0	0
5.56	0.008	0.97	0.96	0.0077	0.0077
5.63	0.008	0.97	0.96	0.0077	0.0077
5.71	0.034	0.96	0.96	0.0326	0.0326
5.80	0.326	0.93	0.92	0.3032	0.2999
5.88	0.511	0.88	0.88	0.4497	0.4497
5.97	0.549	0.82	0.84	0.4502	0.4612
6.06	0.572	0.77	0.80	0.4404	0.4576
6.15	0.621	0.73	0.77	0.4533	0.4782
6.25	0.599	0.70	0.74	0.4193	0.4433
6.35	0.565	0.67	0.69	0.3786	0.3898
6.45	0.561	0.65	0.65	0.3646	0.3646
6.56	0.568	0.63	0.63	0.3578	0.3578
6.67	0.595	0.64	0.64	0.3808	0.3808
6.78	0.621	0.67	0.67	0.4161	0.4161
6.90	0.625	0.72	0.70	0.4500	0.4375
7.02	0.633	0.77	0.74	0.4874	0.4684
7.14	0.565	0.81	0.78	0.4576	0.4407
7.27	0.212	0.83	0.81	0.1759	0.1717
7.41	0.019	0.83	0.765	0.0158	0.0145
7.55	0	0.80	0.60	0	0

TABLE 3. Planck temperatures (K) and WV radiances (W m^{-2} sr^{-1}) from ESOC calibration report and from calculations with WV relative spectral response of Table 2.

T	I_{ESOC}	T	I_{cal}
240	0.6526	240.16	0.6614
241	0.6776	241.16	0.6867
242	0.7033	242.16	0.7127
243	0.7298	243.16	0.7395
244	0.7571	244.16	0.7671
245	0.7851	245.16	0.7955
246	0.8140	246.16	0.8247
247	0.8437	247.16	0.8547
248	0.8742	248.16	0.8855
249	0.9055	249.16	0.9173
250	0.9377	250.16	0.9499
251	0.9708	251.16	0.9833
252	1.0048	252.16	1.0177
253	1.0397	253.16	1.0530
254	1.0756	254.16	1.0893
255	1.1124	255.16	1.1265
256	1.1501	256.16	1.1647
257	1.1889	257.16	1.2038
258	1.2286	258.16	1.2440
259	1.2693	259.16	1.2852
260	1.3111	260.16	1.3274

Calculations were performed for 20 stations. These stations are listed in Table 4, which gives for each of them the radiance value, the zenith angle and the counts of the digital tape. Fig. 3 illustrates the results. Uncertainties in the geographical location of the Meteosat observations and inaccuracies of soundings may be responsible for the scattering of values around the regression line. The number of cases studied was mainly limited by the number of cloudless complete soundings available on the two pictures. The mean line is parallel to the temporary calibration curve obtained with a different method

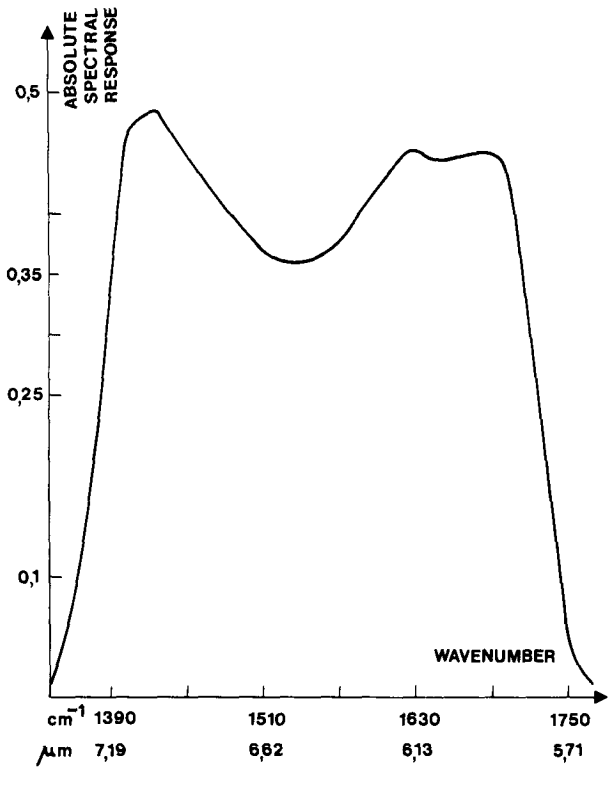

FIG. 2. Apparatus function.

TABLE 4. Calculated radiances and digital counts for the two Meteosat WV pictures (14 July 1978, and 16 July 1978, at 12 GMT).

Date (1978)	Stations	Sec θ	I (W m^{-2} sr^{-1})	Counts
14 July	Ajaccio	1.532	0.99	117
	Belfast	2.160	0.70	77
	Belgrade	1.766	0.91	105
	Bordeaux	1.610	0.88	117
	Brest	1.797	0.64	89
	Camborne	1.870	0.78	113
	Funchal	1.343	1.05	129
	Gibraltar	1.354	1.05	141
	Idris	1.311	1.06	145
	Lisbonne	1.435	1.03	145
	Lyon	1.654	0.80	105
	Malte	1.400	1.08	137
	Nîmes	1.582	0.84	109
	Udine	1.725	0.77	85
16 July	Ajaccio	1.532	0.91	117
	Lisbonne	1.435	1.01	121
	Malte	1.400	1.09	148
	Nîmes	1.582	0.91	109
	Rome	1.550	0.86	109
	Tunis	1.391	1.15	154

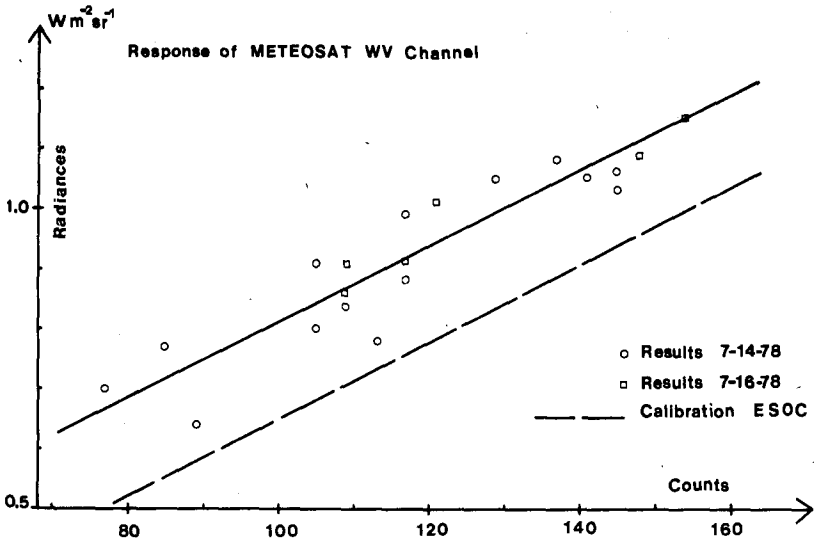

FIG. 3. Response of Meteosat water vapor channel: radiances versus counts.

and published by the European Space Operations Centre (ESOC).

4. Radiance distribution with altitude

Patterns seen in water vapor imagery are not easily correlated with height. In order to determine the altitude of the phenomena observed on these water vapor pictures (14 and 16 July 1978), we looked for the distribution with altitude of the integrated outgoing radiance sensed by the water vapor channel. The function describing the region of the atmosphere from which the radiation originates is the contribution function ψ defined by

$$\psi(\ln P) = \int_{\nu_1}^{\nu_2} g_\nu B_\nu \frac{\partial \tau_\nu}{\partial \ln P} d\nu,$$

where g_ν is the apparatus function in the spectral range of Meteosat WV channel (ν_1,ν_2); B_ν is the Planck blackbody function for the temperature at the pressure level P, τ_ν the transmittance of the absorbing gas between the top of the atmosphere and the pressure level P for the frequency ν. The contribution functions are dependent on the temperature and humidity profiles. For studying the role of these two parameters, we carried out calculations for model atmospheres, which all have the same vertical distribution of temperature and different water vapor profiles.

TABLE 5. Description of the model atmospheres.

	Model atmospheres Secant θ = 1.55; θ = 50°
A	Midlatitude Summer (McClatchey *et al.*, 1972)
C	A + 5% relative humidity between 1000 and 200 mb
D	A − 5% relative humidity between 1000 and 200 mb
E	50% relative humidity between 1000 and 200 mb
F	70% relative humidity between 1000 and 200 mb
H	Same profile as A up to 600 mb 70% relative humidity at 300 mb
J	Same profile as A up to 600 mb 10% relative humidity at 300 mb
K	Same profile as A up to 600 mb 15% relative humidity at 300 mb
L	About 20% between 600 and 250 mb
N	L + 5% relative humidity
O	L − 5% relative humidity

The McClatchey's[5] midlatitude summer model atmosphere seemed suitable to represent points of a picture acquired in July over the occidental part of Europe and Mediterranean Basin. Starting from this basic model (hereafter referred to as MISUM A), we built additional model atmospheres, briefly described in Table 5, for which detailed data are presented in the Appendix (Table A1).

The contribution functions $\psi(\ln P)$ were calculated and Fig. 4 shows these functions for three models: the basic atmosphere (MISUM A), the driest atmosphere (MISUM J), and the wettest atmosphere (MISUM F). The other curves are not presented, for the resulting figure would have been too confused. Complete results are summarized in Table 6, where P_ψ is the pressure level where the maximum contribution to the emitted radiance observed by the WV channel sensor occurs. The drier the atmosphere the lower the layer from which the principal contribution arises and the higher the maximum value of the contribution function ψ. In Fig. 5, the pressure level of the contribution peak versus

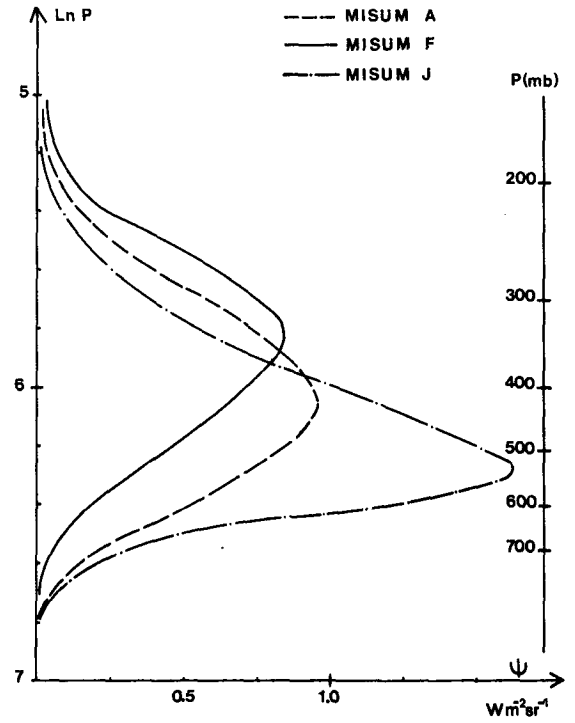

FIG. 4. Contribution functions $\psi(\ln P)$ for three models atmosphere: the basic MISUM A, the driest MISUM J, the wettest MISUM F.

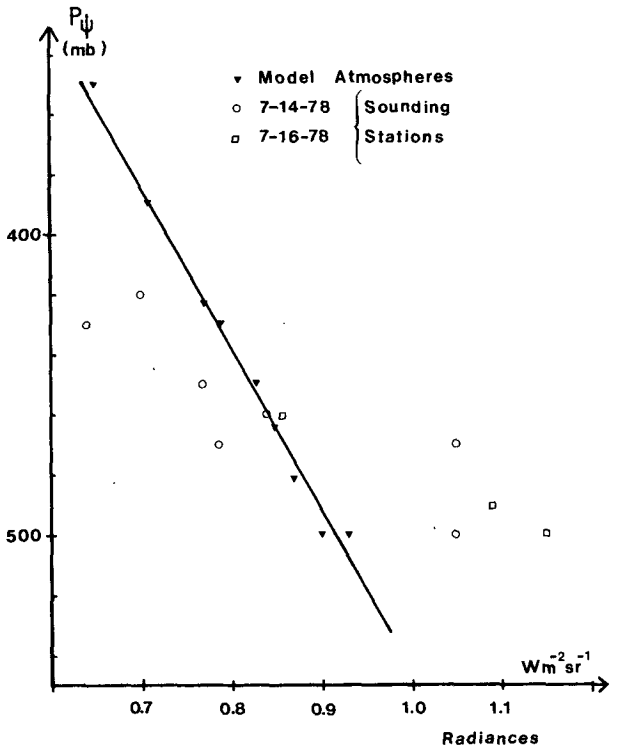

FIG. 5. A plot of the pressure level of the contribution peak P_ψ versus the WV outgoing radiance I.

the outgoing radiance is plotted. It appears in this figure that the relation is linear. This type of variation demonstrates the sensitivity of the altitude of the peak contribution to water vapor distribution, since all the model atmospheres have the same temperature profile.

These results suggest the possibility of deducing the altitude of the phenomena observed on the Meteosat WV images. Similar computations of contribution functions were achieved using the meteorological data acquired from the radiosoundings of the stations situated on the studied pictures (1200 GMT 14 and 16 July 1978). Results obtained are given in the two first columns of Table 7 and the values are plotted in Fig. 5. The range of altitude variation is smaller for the stations than for the model atmospheres. In that case, the two parameters, temperature and humidity profiles, determine the altitude of the peak contribution. To demonstrate the part of temperature, an attempt was made to bring the station values into better agreement with the models. New radiances I' were computed for these stations with the temperature distribution of the model atmospheres, keeping the observed relative humidity profile of each station. New contribution

TABLE 6. Radiances and pressure levels of the peak contribution for model atmospheres.

Model atmospheres	I (W m^{-2} sr^{-1})	P_ψ (mb)
MISUM A	0.79	430
MISUM C	0.77	420
MISUM D	0.83	450
MISUM E	0.71	390
MISUM F	0.65	350
MISUM H	0.67	380
MISUM J	0.98	520
MISUM K	0.90	500
MISUM L	0.87	480
MISUM N	0.85	460
MISUM O	0.93	500

TABLE 7. Radiances and pressure levels of the peak contribution without and with temperature corrections for radiosounding stations.

Date (1978)	Stations	I (W m^{-2} sr^{-1})	P_ψ (mb)	I' (W m^{-2} sr^{-1})	P_ψ' (mb)
14 July	Belfast	0.70	410	0.68	390
	Brest	0.64	430	0.67	380
	Camborne	0.78	470	0.80	420
	Funchal	1.05	500	1.05	530
	Gibraltar	1.05	470	1.02	480
	Nîmes	0.84	460	0.84	460
	Udine	0.77	450	0.78	410
16 July	Malte	1.09	490	1.03	530
	Rome	0.86	460	0.85	460
	Tunis	1.15	500	1.08	530

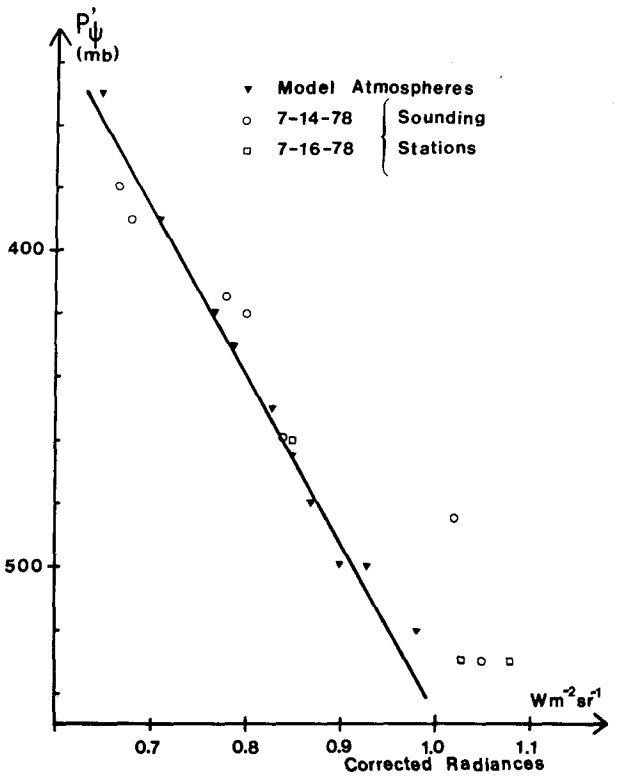

FIG. 6. A plot of the pressure level of the contribution peak P_ψ' versus the temperature corrected WV radiances I'.

functions were obtained from which new pressure levels P_ψ' were extracted. These new values are listed in the two last columns of Table 7.

Fig. 6 represents the values I' plotted versus P_ψ' for the stations together with the results for the model atmospheres. Almost all the points are on the same line and the dispersion around it is much smaller than in Fig. 5. The range of altitude variation for the stations with the temperature correction is of the same order of magnitude as for the model atmospheres. These calculations demonstrated the respective importance of the two parameters temperature and humidity on the altitude of the phenomena observed on WV pictures. But, because of their correlated influence, the relation between radiance and altitude is not obvious in regions where the temperature field shows large variations. It would be possible to use radiance measurements of sounding radiometers such as TIROS-N HIRS/2 to retrieve the temperature profile and infer the altitude of the phenomena observed on water vapor pictures.

5. Precipitable water content

The water vapor quantity related to the radiometric observations is the total precipitable water above given pressure levels.

The relation between the calculated radiance values I and the pressure level of the contribution peak P_ψ in Fig. 5 shows that the maximum emission detected from the WV channel sensor comes mainly from layers extending from 400 to 550 mb. Therefore, we looked for the level above which there is a strong correlation between the water vapor mass and the radiance.

In this aim, water vapor content was calculated above three of the levels included in our model atmospheres between 600 and 500 mb. Results were obtained for the model atmospheres and the sounding stations mentioned above. They are listed in Tables 8a and 8b, where I is the radiance (in W m^{-2} sr^{-1}); e is the total water vapor content in precipitable centimeters; e_1, e_2, e_3 are the water vapor mass above the three levels (600, 570 and 530 mb, respectively).

Fig. 7 represents graphically the results for the water vapor mass above 600 mb. The correlation

TABLE 8. Precipitable water vapor contents: total (e), and above the three levels: 600 mb (e_1), 570 mb (e_2) and 530 mb (e_3).

(a) Model atmospheres

Model atmospheres	I (W m^{-2} sr^{-1})	e (cm)	e_1 (cm)	e_2 (cm)	e_3 (cm)
MISUM A	0.79	4.71	0.44	0.33	0.24
MISUM C	0.77	5.11	0.51	0.38	0.28
MISUM D	0.83	4.28	0.37	0.28	0.20
MISUM E	0.71	5.02	0.67	0.51	0.28
MISUM F	0.65	6.02	0.96	0.74	0.56
MISUM H	0.67	4.89	0.63	0.51	0.40
MISUM J	0.98	4.53	0.26	0.16	0.10
MISUM K	0.90	4.58	0.31	0.21	0.14
MISUM L	0.87	3.03	0.28	0.21	0.15
MISUM N	0.85	3.29	0.33	0.24	0.18
MISUM O	0.93	2.76	0.24	0.17	0.13

(b) Sounding stations

Date (1978)	Stations	I (W m^{-2} sr^{-1})	e (cm)	e_1 (cm)	e_2 (cm)	e_3 (cm)
14 July	Ajaccio	0.99	3.89	0.27	0.20	0.14
	Belfast	0.70	3.52	0.43	0.35	0.27
	Belgrade	0.91	4.76	0.23	0.13	0.08
	Bordeaux	0.88	4.60	0.29	0.19	0.13
	Brest	0.64	4.19	0.69	0.53	0.39
	Camborne	0.78	4.05	0.33	0.23	0.15
	Funchal	1.05	2.45	0.15	0.11	0.08
	Gibraltar	1.05	3.53	0.31	0.22	0.14
	Idris	1.06	3.29	0.23	0.17	0.12
	Lisbonne	1.03	2.43	0.18	0.14	0.11
	Lyon	0.80	3.16	0.39	0.29	0.21
	Malte	1.08	1.73	0.22	0.16	0.11
	Nîmes	0.84	5.02	0.38	0.27	0.18
	Udine	0.77	4.93	0.35	0.28	0.20
16 July	Ajaccio	0.91	4.74	0.32	0.25	0.20
	Lisbonne	1.01	2.39	0.29	0.18	0.11
	Malte	1.09	3.96	0.26	0.17	0.11
	Nîmes	0.91	2.94	0.32	0.27	0.23
	Rome	0.86	5.23	0.36	0.28	0.22
	Tunis	1.15	2.99	0.22	0.11	0.09

obtained confirms that the larger the radiance the drier the atmosphere above this level. For radiance values in the range of 0.7 to 1.3 W m^{-2} sr^{-1}, the water vapor mass above 600 mb varies from 0.2 to 1.0 cm precipitable water vapor content. Dispersion around the regression curve can be easily explained by uncertainties on the humidity profile determination. Similar correlations were found above the two upper levels 570 and 530 mb. The scatter of the values is slightly smaller than at the 600 mb level. Fig. 8 gathers the curves of water vapor mass above the three levels plotted versus the radiance I. Only the regression curves have been drawn on this figure for the sake of clearness.

6. Conclusion

An accurate transmittance and radiance model has been used to obtain the response of the Meteosat water vapor channel by comparing the radiance calculated from atmospheric data with the numerical values extracted in clear-sky conditions on an image at specific geographical points. The linear relation between radiances and digital counts obtained is parallel to the ESOC calibration line; the range is shifted about 40 counts for the same value of the radiance. Later this year a moon calibration project will be realized by ESOC and this will lead to a new comparison.

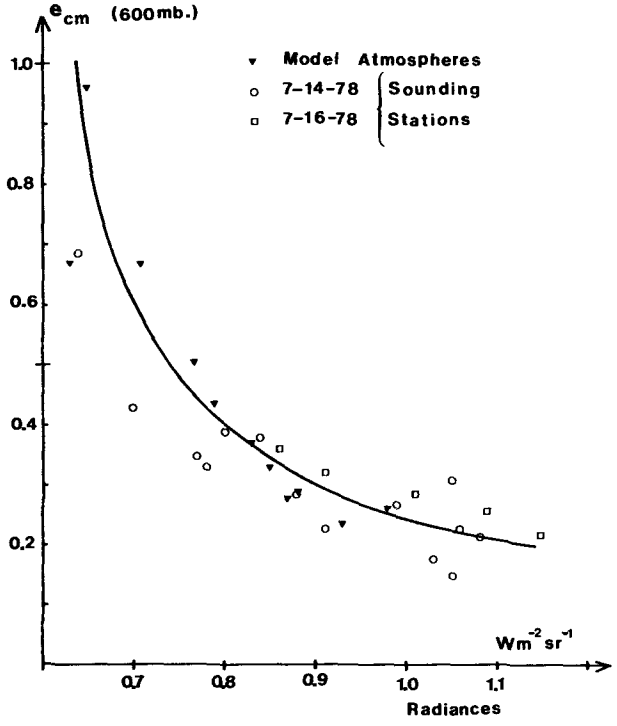

FIG. 7. Variation of radiances I with the precipitable water content e_1 above the 600 mb level.

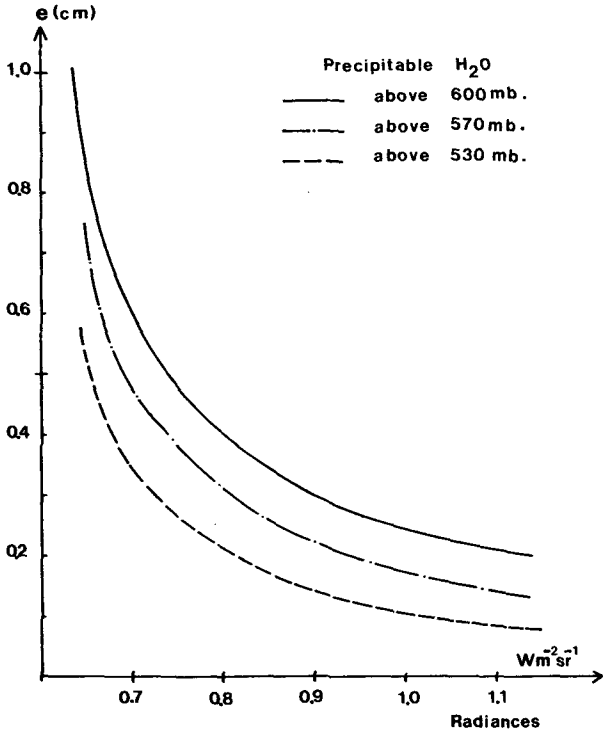

FIG. 8. Curves showing the water vapor mass above three levels (600 mb, 570 mb, 530 mb) plotted versus the radiances I.

The determination of the altitude of the phenomena observed on WV Meteosat imagery was realized by examining the behavior of the contribution functions. The altitude variation for actual meteorological data, associated with the Meteosat pictures chosen, is about 100 mb in the vicinity of 500 mb. This relatively small range was explained by the variability of the temperature profile from one sounding to another, in summer and in the geographical region studied. The altitude range of the phenomena observed may be different at other latitudes and for various seasons. Because of the uncertainties due to temperature variation, the actual altitude range of the phenomena observed cannot be established using only water-vapor channel data.

It was possible to infer a quantitative correlation beween the radiance and the water vapor mass above a given pressure level. This level appears to be as low as 600 mb in the cases studied from Meteosat water vapor pictures.

The distribution pattern of precipitable water content above ~600 mb could be deduced from water vapor Meteosat imagery. Analyses of successive pictures will provide spatial and temporal evolution of these patterns.

Acknowledgments. The authors wish to thank A. Semery who designed the navigation programme.

APPENDIX

Model Atmospheres Used for the Computations

TABLE A1. Letters indicate the name of the model atmospheres, P (mb) is the pressure level, T (K) the temperature and r the mixing ratio (g g^{-1}).

P	T	A	C	D	E	F	H	J	K	L	N	O
(mb)	(K)	r (g g^{-1})	r (g g^{-1})	r (g g^{-1})	r (g g^{-1})	r (g g^{-1})	r (g g^{-1})	r (g g^{-1})	r (g g^{-1})	r (g g^{-1})	r (g g^{-1})	r (g g^{-1})
1018	294.0	1.2 E-02	1.27 E-02	1.12 E-02	1.2 E-02	1.2 E-02	1.2 E-02	1.2 E-02	1.2 E-02	7.74 E-03	8.19 E-03	7.23 E-03
789.7	284.4	5.6 E-03	6.12 E-03	5.08 E-03	5.6 E-03	7.23 E-03	5.6 E-03	5.6 E-03	5.6 E-03	3.61 E-03	3.95 E-03	3.28 E-03
693.8	277.8	3.5 E-03	3.86 E-03	3.11 E-03	3.76 E-03	5.26 E-03	3.5 E-03	3.5 E-03	3.5 E-03	2.26 E-03	2.49 E-03	2.01 E-03
608.1	271.4	2.0 E-03	2.28 E-03	1.74 E-03	2.70 E-03	3.78 E-03	2.0 E-03	2.0 E-03	2.0 E-03	1.29 E-03	1.47 E-03	1.12 E-03
569.7	268.3	1.6 E-03	1.83 E-03	1.37 E-03	2.30 E-03	3.23 E-03	1.85 E-03	1.3 E-03	1.4 E-03	1.03 E-03	1.18 E-03	8.84 E-04
531.3	265.0	1.3 E-03	1.49 E-03	1.10 E-03	1.96 E-03	2.75 E-03	1.6 E-03	7.4 E-04	8.8 E-04	8.39 E-04	9.61 E-04	7.10 E-04
497.0	261.9	1.0 E-03	1.16 E-03	8.41 E-04	1.59 E-03	2.30 E-03	1.45 E-03	5.0 E-04	6.4 E-04	6.45 E-04	7.48 E-04	5.43 E-04
462.7	258.6	8.0 E-04	9.33 E-04	6.66 E-04	1.25 E-03	1.80 E-03	1.25 E-03	3.1 E-04	4.4 E-04	5.16 E-04	6.02 E-04	4.30 E-04
432.2	255.6	6.5 E-04	7.61 E-04	5.38 E-04	1.12 E-03	1.56 E-03	1.05 E-03	2.25 E-04	3.3 E-04	4.19 E-04	4.91 E-04	3.47 E-04
401.6	251.8	5.0 E-04	5.85 E-04	4.15 E-04	8.50 E-04	1.19 E-03	9.0 E-04	1.7 E-04	2.5 E-04	3.23 E-04	3.77 E-04	2.68 E-04
347.3	244.9	3.2 E-04	3.62 E-04	2.78 E-04	4.90 E-04	8.0 E-04	6.8 E-04	1.05 E-04	1.65 E-04	2.06 E-04	2.34 E-04	1.79 E-04
299.2	238.0	1.8 E-04	2.13 E-04	1.47 E-04	2.50 E-04	4.58 E-04	4.25 E-04	6.4 E-05	1.0 E-04	1.16 E-04	1.37 E-04	9.48 E-05
256.8	231.2	8.0 E-05	9.23 E-05	6.77 E-05	1.23 E-04	1.73 E-04	2.4 E-04	2.7 E-05	4.5 E-05	5.16 E-05	5.95 E-05	4.37 E-05
219.9	224.2	2.8 E-05	3.43 E-05	2.18 E-05	6.29 E-05	6.29 E-05	1.1 E-04	1.25 E-05	2.25 E-05	1.81 E-05	2.21 E-05	1.41 E-05
188.2	217.8	1.4 E-05	1.73 E-05	1.08 E-05	1.40 E-05	1.4 E-05	2.2 E-05	8.0 E-06	1.4 E-05	9.03 E-05	1.12 E-05	6.97 E-06
137.8	216.0	5.5 E-06	5.5 E-06	5.5 E-06	5.5 E-06	5.5 E-06	5.5 E-06	5.5 E-06	5.5 E-06	3.55 E-06	3.55 E-06	3.55 E-06
100.7	216.0	3.35 E-06	3.35 E-06	3.35 E-06	3.35 E-06	3.35 E-06	3.35 E-06	3.35 E-06	3.35 E-06	2.16 E-06	2.16 E-06	2.16 E-06
62.8	217.7	2.3 E-06	2.3 E-06	2.3 E-06	2.3 E-06	2.3 E-06	2.3 E-06	2.3 E-06	2.3 E-06	1.48 E-06	1.48 E-06	1.48 E-06
39.1	221.5	2.8 E-06	2.8 E-06	2.8 E-06	2.8 E-06	2.8 E-06	2.8 E-06	2.8 E-06	2.8 E-06	1.80 E-06	1.80 E-06	1.80 E-06
24.3	226.3	3.0 E-06	3.0 E-06	3.0 E-06	3.0 E-06	3.0 E-06	3.0 E-06	3.0 E-06	3.0 E-06	1.94 E-06	1.94 E-06	1.94 E-06
5.18	250.5	3.0 E-06	3.0 E-06	3.0 E-06	3.0 E-06	3.0 E-06	3.0 E-06	3.0 E-06	3.0 E-06	1.94 E-06	1.94 E-06	1.94 E-06

REFERENCES

Chedin, A., N. Husson, N. A. Scott and D. Gautier, 1978: ν_4 band of methane ($^{12}CH_4$ and $^{13}CH_4$). Line parameters and evaluation of Jovian atmospheric transmission at 7.7 μm. *J. Mol. Spectrosc.*, **71**, 343–368.

Möller, F., 1961: Atmospheric water vapor measurements at 6–7 μm from a satellite. *Planetary Space Sci.*, **5**, 202–206.

Raschke, E., and W. R. Bandeen, 1967: A quasi-global analysis of tropospheric water vapor content from TIROS-IV radiation data. *J. Appl. Meteor.*, **6**, 468–481.

Rodgers, E. B., V. V. Salomonson and H. Lee Kyle, 1976: Upper tropospheric dynamics as reflected in Nimbus-4 THIR 6–7 μm data. *J. Geophys. Res.*, **81**, 5749–5758.

Roulleau, M., 1978: *Remote Sensing of the Atmosphere: Inversion Methods and Applications*. Elsevier, 149–159.

Scott, N. A., 1974: A direct method of computation of the transmission function of an inhomogeneous gaseous medium. I: Description of the method. *J. Quant. Spectrosc. Radiat. Transfer*, **14**, 691–704.

Steranka, J., L. J. Allison and V. V. Salomonson, 1973: Application of Nimbus-4 THIR 6–7 μm. Observations to regional and global moisture and wind field analysis. *J. Appl. Meteor.*, **12**, 386–395.